RSC Advances

ROYAL SOCIETY OF CHEMISTRY

www.rsc.org/advances

Journal Name

ARTICLE

Nickel clusters grown on three-dimensional graphene oxide-multi-wall carbon nanotubes as electrochemical sensing platform for luteolin at picomolar level

Received ooth January 20xx,
Accepted ooth January 20x

DOI: 10.1039/x0xx00000x

www.rsc.org/

Taotao Yang [a,b,†], Yansha Gao [a,†], Jingkun Xu [a,*], Limin Lu [b,*], Yuanyuan Yao [a,†], Zifei Wang [a,†], Xiaofei Zhu [a,†], Huakun Xing [a,†]

This study focuses on enhancing the catalytic activity of metallic Ni by using various nanostructured carbon materials, including 1D multi-wall carbon nanotubes (MWCNTs), 2D graphene oxide (GO) and graphene (GR), and 3D graphene oxide-multi-wall carbon nanotubes (GO-MWCNTs) as supporting matrixs for the fabrication of electrochemical sensor for detecting the flavonoid luteolin. Ni clusters were prepared by a facile electrochemical approach and the metallic Ni on various carbon supports exhibited different morphology, which were characterized by scanning electron microscopy (SEM) and Raman spectra. The electrocatalytic performance of Ni-based materials towards luteolin oxidation was studied by cyclic voltammetry (CV) and differential pulse voltammetry (DPV). It was found that Ni cluster supported on GO-MWCNTs (Ni/GO-MWCNTs) was profoundly superior to other carbon materials, with a greatly enhanced current. This is attributed not only to the excellent electric conductivity and large surface-to-volume ratio of Ni/GO-MWCNTs, but also to the unique 3D carbon nanostructure that facilitates the easy access of electrolyte and analyte to the modified electrode surface and promotes the reaction kinetics. Under the optimal conditions, the anodic peak current was linear to the concentration of luteolin in the range from 1 pM to 15 μM with the detection limit of 0.34 pM (S/N = 3). The good analytical performance, low cost and straightforward preparation method made this novel electrode material promising for the development of effective luteolin sensor.

1 Introduction

Luteolin (3′, 4′, 5, 7-tetrahydroxyflavone), an important member of the flavonoid family, has been widely distributed in various vegetables and fruits, especially in drugs. Recent studies have shown that this compound has many beneficial effects on human health, including biochemical and pharmacological effects, anti-

inflammatory, anti-bacterial, anti-oxidant, anti-viral, anti-carcinogenic, anticancer activity, cataract prevention, cardiovascular protection, anti-ulcer effects, anti-inammatory effects and anti-allergic properties.[1,2] Luteolin was also found to have pro-oxidant effects, possibly promoting oxidative damage to DNA, lipids, proteins, and carbohydrates.[3,4] In addition to these activities, several epidemiological studies suggested that a high consumption of luteolin is inversely related to the risk of cardiovascular diseases.[5-7] Thus, it is necessary to establish a rapid, simple and effectivemethod for the determination of luteolin.

So far, several techniques have been utilized in the determination of luteolin, including high-performance liquid chromatography,[8,9] liquid chromatography-mass spectrometry,[10,11] spectrophotometry,[12] capillary electrophoresis,[13] and gas chromatography,[14] etc. However, these techniques are time consuming, expensive or require complicated preconcentration, which hamper their further application. In contrast to these methods, electrochemical methods are preferable and interesting because of the advantages of rapidity, low cost, simplicity and high sensitivity for the determination of phenolic compounds.[15] Luteolin is an electroactive compound because of the catechol group on the B ring (3',4'-dihydroxyl) and the development and application of electrochemical sensors and methods for the determination of luteolin has attracted widespread attention in recent years.[16-18] However, luteolin exhibits slow electron transfer at bare glass carbon electrodes, which leads to low sensitivity.[19,20] Therefore, some functional materials should be synthesized to develop a sensitive electrochemical method for its detection.

Hierarchical micro- and nanostructures of inorganic materials have been explored extensively for the fundamental scientific and technological interest in accessing new classes of functional materials with unprecedented properties and applications.[21] As one of the interesting metallic nanomaterials, hierarchical Ni particles have attracted considerable attention due to diverse promising applications in the fields of electrocatalysis, rechargeable batteries, superconducting devices, and so on.[22-24] Over the past decades, various strategies such as magnetic self-assembly process,[25] chemical reduction in the liquid phase,[26] and a template- and surfactant-free strategy,[27] were used to prepare different hierarchical Ni structures. However, these methods always require complex manipulation process, toxic reducing agents or long reaction time. So there still remains a need to develop new strategies for constructing highly active Ni-based materials with superior catalytic property.

Recently, preparing micro- and nano-composites involving highly conductive nanocarbon materials has been proved to be effective for a high performance Ni-based electrode.[28] As a support matrix, nanocarbon materials have several genuine advantages. First, carbon nanotubes (CNTs), graphene oxide (GO) and graphene (GR) have large specific surface areas which can achieve a high dispersion of Ni and improve the electrocatalytic activity of Ni materials. Moreover, the locally conjugated structure endows them with enhanced adsorption capacities towards substrates in the catalytic reaction. Second, the superior electron mobility of CNTs and GR facilitates the electron transfer during the catalytic reactions, improving their catalytic activity.[29,30] Third, they also have high chemical, thermal, optical and electrochemical stabilities, which can possibly improve the lifetime of catalysts.[31] In most cases, however, the excellent properties of CNTs and GR are not revealed in practical applications because they tend to irreversibly aggregate during the fabrication process, resulting in significantly reduced surface areas.[32] This stacking thereby causes inferior mass transport capabilities and renders a substantial number of active sites inaccessible to reactants. In this aspect, several research groups have made outstanding achievements.[33,34] They demonstrated that GO can absorb on the CNTs through the strong π-π interaction to form macroscopic three dimensional hybrid structures, where GO served as a superior dispersant to disperse CNTs and prevented their aggregation. The composite consisting of CNTs and GO exhibited enhanced electronic and catalytic activity, which can

be used for construction of electrochemical sensor with better performances.

In this study, 3D graphene oxide-multi-wall carbon nanotubes （GO-MWCNTs） nanocomposite was prepared by sonication methods without assistance of any surfactant. Uniform Ni clusters were further decorated on GO-MWCNTs (Ni/GO-MWCNTs) by electrochemical deposition method. The 3D microporous GO-MWCNTs with interconnected structure as a supporting matrix for Ni clusters provided enhanced surface area for electron transfer for redox reactions of luteolin. Furthermore, the 3D Ni/GO-MWCNTs has been leading to a high-performance luteolin sensor with a linear detection range of 1 pM-15 μM and detection limit of 0.34 pM (S/N = 3), which is much lower than that based on Ni/GR (167 nM), and Ni/MWCNTs (0.34 nM). 3D Ni/GO-MWCNTs composite provides new avenues for design of high performance electrode materials for luteolin sensing.

2 Experimental

2.1. Reagents

Luteolin was obtained from Aldrich. Luteolin stock solution (0.01 M) was prepared with absolute ethanol and stored at 277-281 K. GO was purchased from Nanjing XFNANO Materials Tech Co., Ltd. MWCNTs (purity > 95%) were purchased from Shenzhen Nanotech Port Co. Ltd. $NiCl_2$ was purchased from Sinopharm Chemical Reagent Co., Ltd. The supporting electrolyte was phosphate buffer solution (PBS) prepared with 0.1 M NaH_2PO_4 and 0.1 M Na_2HPO_4. All these were used as received without further purification and doubly distilled water was used throughout the experiments.

2.2. Apparatus

Cyclic voltammetry (CV) and differential pulse voltammetry (DPV) measurements were carried out on a CHI 660D electrochemical workstation (Shanghai, China).The electrochemical properties of luteolin were measured by CV in a standard three-electrode cell(10 mL). A saturated calomel electrode (SCE) was used as the reference electrode and a platinum wire as the counter electrode. A glassy carbon electrode (GCE) with a geometical area of 0.07065 cm^2, bare or modified, was used as working electrode. The DPV were carried out to obtain a calibration curve with the parameters of increment potential, 0.004 V; pulse amplitude, 0.05 V; pulse width, 0.05 s; sample width, 0.0167 s; pulse period, 0.2 s; quiet time, 2 s. Chronocoulometry were performed to determine the electrochemically effective surface areas of the bare and modified GCE. Electrochemical impedance spectroscopy (EIS) was performed in 5.0 mM $K_3Fe(CN)_6/K_4Fe(CN)_6$ (1:1) mixture with 0.1 M KCl at the formal potential of the 180 mV using alternating voltage of 5.0 mV. The frequency range was from 0.1 Hz to 10 kHz. Scanning electron microscopy (SEM) analysis was performed using a Hitachi S-3000 N scanning electron microscope. Raman spectroscopy (Renishaw in Via 2000) was used to analyze the samples using a 514 nm Ar laser. Electrolyte solutions were deoxygenated by purging pure nitrogen (99.99%) for 10 minutes prior to electrochemical experiments. All potentials were measured and reported versus the SCE and all experiments were carried out at room temperature.

2.3. Fabrication of different modified electrodes

GO (1.0 mg) was dispersed into 5.0 mL doubly distilled water and sonicated for 2 h to yield a yellow-brown dispersion. Then 5.0 mg MWCNTs was added into the homogeneous GO dispersion and sonicated until a homogeneous black suspension was obtained.

Prior to coating the electrode, the glassy carbon electrode (GCE) surface was polished with 0.05 μm Al_2O_3 slurry until visibly lustrous, rinsed thoroughly with double distilled water, then it was ultrasonically cleaned with doubly distilled water, absolute ethanol and doubly distilled water each for 5 min, respectively, and dried in air before use. 6 μL of the GO-MWCNTs suspension was transferred on the surface of GCE and dried at room temperature. Then, the GO-MWCNTs/GCE was placed in a solution containing 0.02 mM $NiCl_2$ with 1 M

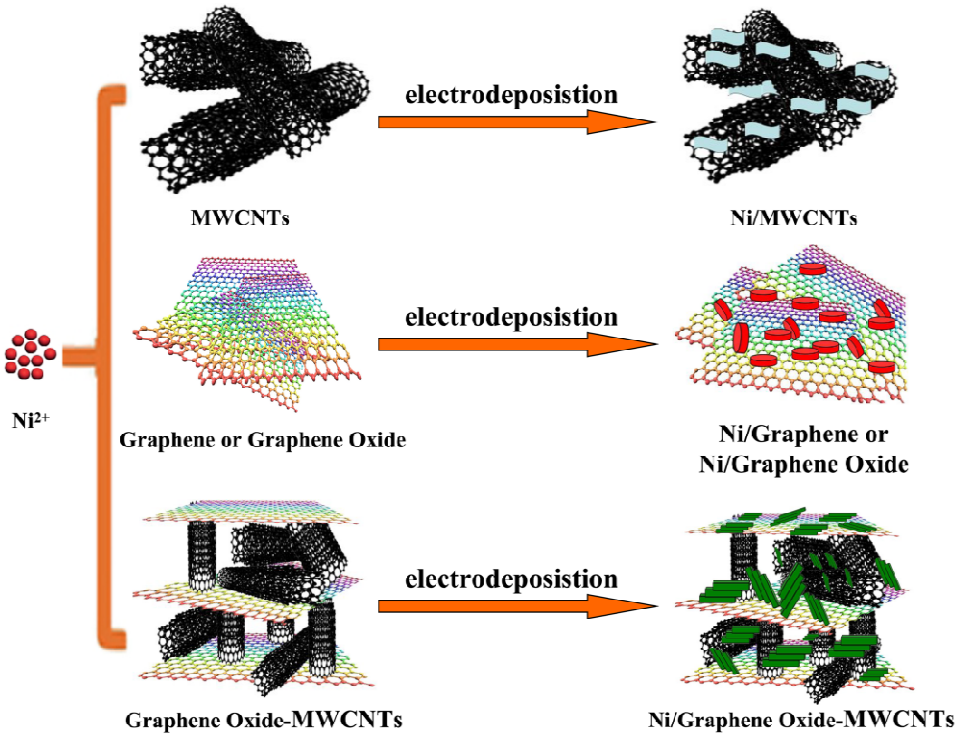

Scheme 1. The preparation process of Ni/MWCNTs/GCE, Ni/GO/GCE, Ni/GR/GCE and Ni/GO-MWCNTs/GCE.

H_2SO_4 and controlled electrodeposition of Ni was performed at -0.2 V for 6 s to obtain Ni/GO-MWCNTs/GCE. For the comparison, GO/GCE, MWCNTs/GCE, Ni/GO/GCE, Ni/GR/GCE, Ni/MWCNTs/GCE and Ni/GCE were fabricated in a similar method. The Ni/GR/GCE was obtained by the electrochemical reduction of the GO/GCE by applying a constant potential of -1.0 V for 400 s before controlled electrodeposition of Ni. Scheme 1 shows the procedure for preparing Ni/MWCNTs, Ni/GO, Ni/GR and Ni/GO-MWCNTs modified electrodes.

3. Results and discussion

3.1. Characterization of composites film

In this work, four kinds of nanostructured carbon materials (1D MWCNTs, 2D GO, GR and 3D GO-MWCNTs) were used as supporting matrixs to prepare Ni-based materials by using electrodeposition method. Their effects on the resultant Ni-based materials morphology were studied by SEM. For Ni/MWCNTs (Fig. 1a), bulk Ni was observed on the MWCNTs. While for Ni/GO (Fig. 1b) and Ni/GR (Fig. 1c), Ni showed a uniformly distributed coin-like morphology. For the 3D GO-MWCNTs substrate, it can be seen that GO could absorb on the MWCNTs through the strong π-π interaction, forming the GO-MWCNTs microporous 3D porous structures (Fig. 1d). After controlled electrodeposition of Ni on 3D substrate, the obtained Ni/GO-MWCNTs (Fig. 1e) showed a more uniform surface topography than 1D Ni/MWCNTs and 2D Ni/GO, Ni/GR. Moreover, high-resolution SEM images in Fig. 1f-h revealed that the overall morphology of Ni/GO-MWCNTs exhibited a 3D coil-like structure architecture, which was assembled by several pieces of Ni sheets. This 3D

porous structure could significantly increase the effective electrode surface and facilitate the diffusion of the analytes into the film.

Raman spectra of the Ni/GO-MWCNTs, Ni/GO, Ni/GR and Ni/MWCNTs are shown in Fig 2. The D and G bands were observed in all samples in the range of 1000 - 2000 cm^{-1}. The D band could be employed to measure the defects of the sample while the G band could be used to study sp^2 carbon networks of the sample. It is obvious that the G band of Ni/GO-MWCNTs (1578 cm^{-1}) shows a visible red-shift in comparison with that of Ni/GO (1606 cm^{-1}) and Ni/MWCNTs (1582 cm^{-1}),[35] suggesting that a larger size of the in-plane sp^2 domains are obtained by hybriding GO and MWCNTs, which further confirmed the truth of π-π stacking interaction between GO and MWCNTs.[36,37] Moreover, the D/G intensity ratio (I_D/I_G) of the Ni/GO-MWCNTs (1.15) washigher compared with those of Ni/GR (1.08), Ni/GO (1.01) andNi/MWCNTs (0.145). These changes indicate the formation of Ni/GO-MWCNTs.[38]

The EIS analysis is one of the principal methods for examining the fundamental behavior of electrode materials for electrochemical. The value of the electrodetransfer resistance (Ret), which depends on the dielectric and insulating features at the electrode/electrolyte interface, can beobtained from the semicircle diameters of the Nyquist plot. Fig. 3 presents the representative impedance spectrum of the bare GCE (a), GO/GCE (b), MWCNTs/GCE (c), GO-MWCNTs/GCE (d) and Ni/GO-MWCNTs/GCE (e) in 5.0 mM K3Fe(CN)6/K4Fe(CN)6 (1:1) containing 0.1 M KCl. Compared with bare GCE (a), the semicircle of GO/GCE (b) dramatically increases, suggesting that GO acted as an insulating layer which made the interfacial charge transfer difficult. When MWCNTs was modified onto the GCE(c), the semicircle decreases distinctively relative to the bare GCE (a), which is ascribed to the significantly conductivity of MWCNTs. The semicircle of GO-MWCNTs/GCE is larger than that of MWCNTs/GCE butsmaller than that of GO/GCE, suggesting that MWCNTs were successfully dispersed by GO. After the deposition of Ni, the obtained Ni/GO-MWCNTs/GCE exhibited a markedly decreased Rct value, manifesting that Ni with good electrical conductivity were successfully deposited and they can provide necessary conductive pathways to assist the charge/electron transfer.

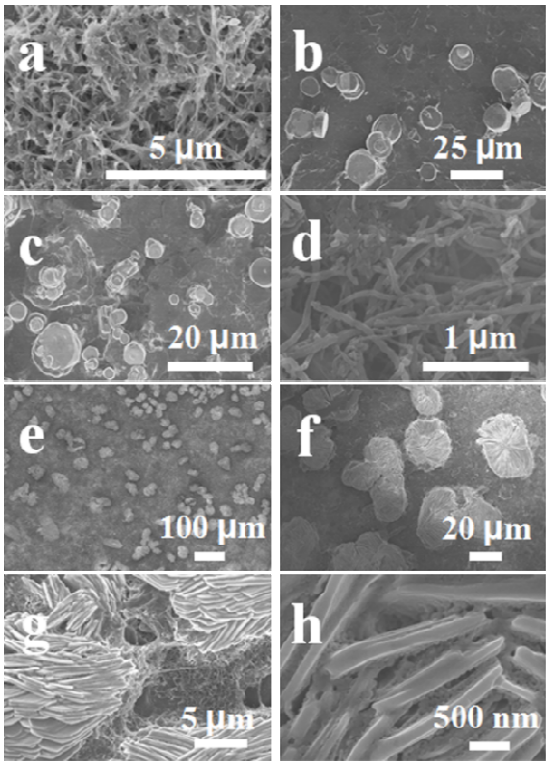

Fig. 1 Scanning electron microscope images of Ni/MWCNTs (a), Ni/GO (b), Ni/GR (c), GO/MWCNTs (d), Ni/GO-MWCNTs (e-h).

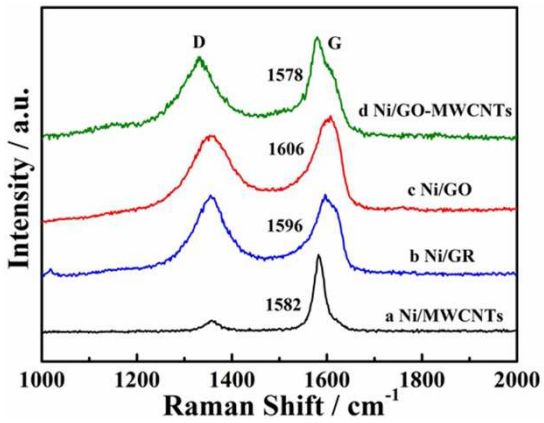

Fig. 2 Raman spectra of Ni/MWCNTs (a), Ni/GR (b), Ni/GO (c), Ni/GO-MWCNTs (d).

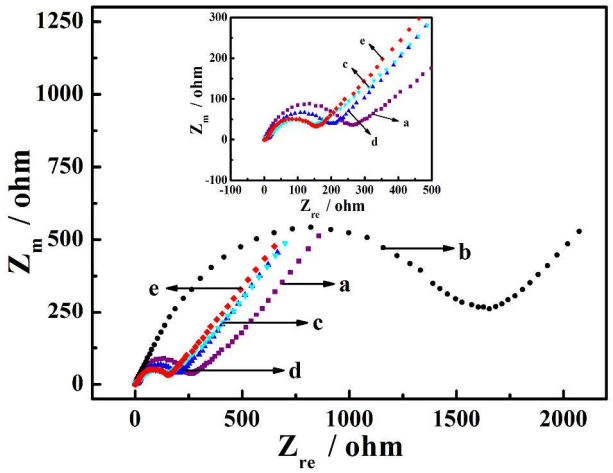

Fig. 3 The representative impedance spectrum of the bare GCE (a), GO/GCE (b), MWCNTs/GCE (c), GO-MWCNTs/GCE (d), Ni/GO-MWCNTs/GCE (e) in 5.0 mM $K_3Fe(CN)_6/K_4Fe(CN)_6$ (1:1) containing 0.1 M KCl.

3.2. Electrochemical behaviors of luteolin at various electrodes

SEM results indicate that substrates material has an important effect on the Ni morphology. It is supposed that the substrates material might affect the electrocatalytic activity of Ni-based materials, then the electrocatalytic activity of different dimensions carbon materials toward luteolin was investigated. As can be observed from Fig. 4A, when 100 μM luteolin was added into pH 3.0 PBS, luteolin showed poor redox current peaks at the bare GCE (a) and GO/GCE (b) within the potential window from 0 to 0.80 V, which might be due to the sluggish electron transfer of bare GCE and poor conductivity of GO. Larger oxidation peak current can be observed on GR/GCE (c) and MWCNTs/GCE (d), ascribing to the excellent electrical conductivity and large surface area properties of GR and MWCNTs. Compared with the 2D GO/GCE , GR/GCE and 1D MWCNTs/GCE, the redox peak currents show a remarkable increase on the 3D GO-MWCNTs/GCE (e). These results might be attributed to the interconnected 3D nanostructure of GO-MWCNTs and the synergistic effect of MWCNTs and GO sheets, in which GO provides a large specific surface area to assisted the dispersion of pristine MWCNTs and hastens the electron transfer process as well as improving the mass transfer kinetics.

After deposition of Ni on different substrates, the electrochemical behavior of Ni-based electrodes was also investigated. As shown in Fig. 4B, the peak intensity of the current was increased in the following order: Ni/GCE (f) < Ni/GO/GCE (g) < Ni/GR/GCE (h) < Ni/MWCNTs/GCE (i) < Ni/GO-MWCNTs/GCE (j). This revealed that 3D Ni/GO-MWCNTs as Ni support matrix showed better catalytic activity than 1D MWCNTs, 2D GO and GR. The excellent electrochemical catalytic properties of Ni/GO-MWCNTs can be summarized in the following aspects: firstly, interconnected 3D network of GO-MWCNTs has good electrical conductivity and large specific surface area, which can provide an excellent microenvironment for the catalytic oxidation of luteolin. Secondly, the uniform Ni clusters decorated on GO-MWCNTs would provide more active sites for the catalytic oxidation reaction and greatly increase the electrocatalytic activity.

3.3. Optimization of the experimental conditions

3.3.1 Effect of pH

The influence of pH values on the redox reaction of luteolin on the Ni/GO-MWCNTs/GCE was studied in the pH range from 2.0 to 8.0 using 0.1M PBS. As can be seen in Fig. 5A, the reduction peak current of luteolin increases with increasing pH value when it reached 3.0, and then decreases when the pH increased further. Considering the sensitivity for determining luteolin, pH 3.0 was chosen for the subsequent analytical experiments. Moreover, with pH value of the solution increasing, the reduction peak potential (E_p) shifts negatively, indicating that protons have taken part in the electrode reaction process of luteolin. It is found that the value of the reduction peak potential changed linearly with pH values, and that it obeys the following equation: E_p = - 0.058 pH + 0.772 (R^2 = 0.9989) (shown in Fig. 5B). The absolute value of the

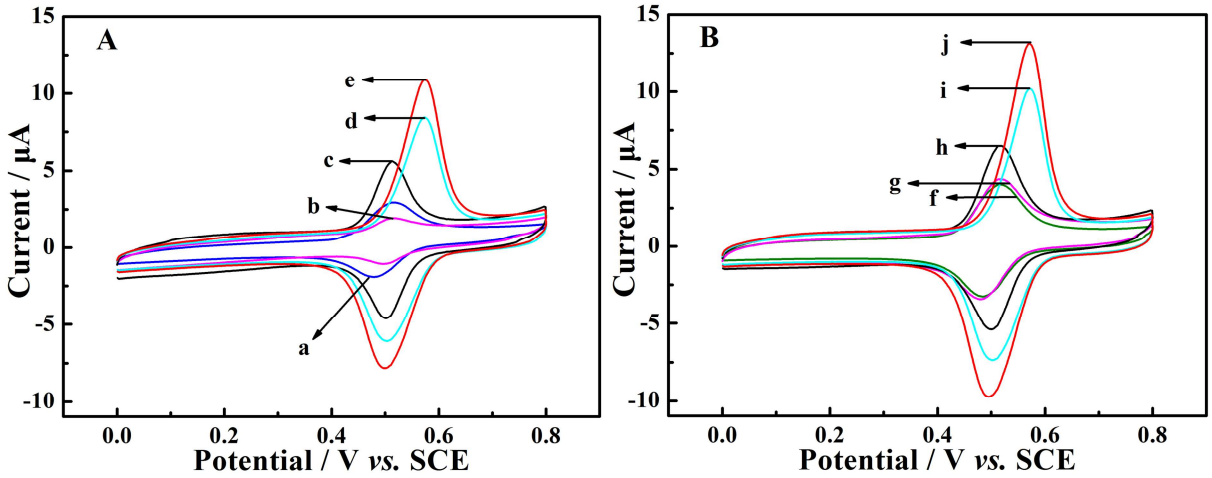

Fig. 4 Cyclic voltammograms: (A) for bare GCE (a), GO/GCE (b), GR/GCE (c), MWCNTs/GCE (d), GO-MWCNTs/GCE (e); (B) for Ni/GCE (f), Ni/GO/GCE (g), Ni/GR/GCE (h), Ni/MWCNTs/GCE (i), Ni/GO-MWCNTs/GCE (j) in the presense of 100 μM luteolin in 0.1 M PBS (pH 3.0), Scan rate: 50 mV s^{-1}.

slope is approximately close to the theoretical value of 59 mV pH^{-1}, indicating that the number of proton and electron involved in the electrochemical redox process of luteolin is equal.[39]

3.3.2 Influence of scan rate on the peak currents of luteolin

The influence of scan rate on the electrochemical response of 50 μM luteolin in 0.1 M PBS (pH 3.0) at Ni/GO-MWCNTs/GCE was investigated in the range of 10 - 450 mV s^{-1} by CV (Fig. 6). The anodic peak currents (I_{pa}) and cathodic peak currents (I_{pc}) increased linearly with the scan rates. The linear relationship of I_p and v can be expressed in the following equations: I_{pa} (μA) = 0.3795 v - 4.996 (R^2 = 0.9987) and I_{pc} (μA) = -0.3203 v + 5.814 (R^2 = 0.9974), respectively. These results indicated that the electron-transfer reaction of luteolin at the Ni/GO-MWCNTs/GCE was a predominantly adsorption-controlled process.

In addition, as shown in Fig. 6C, with increasing scan rate, the anode (E_{pa}) and cathode (E_{pc}) peak potential have a linear relationship with the Napierian logarithm of scan rate (ln v). In the scan rates ranging from 10 to 450 mV s^{-1}, the linear

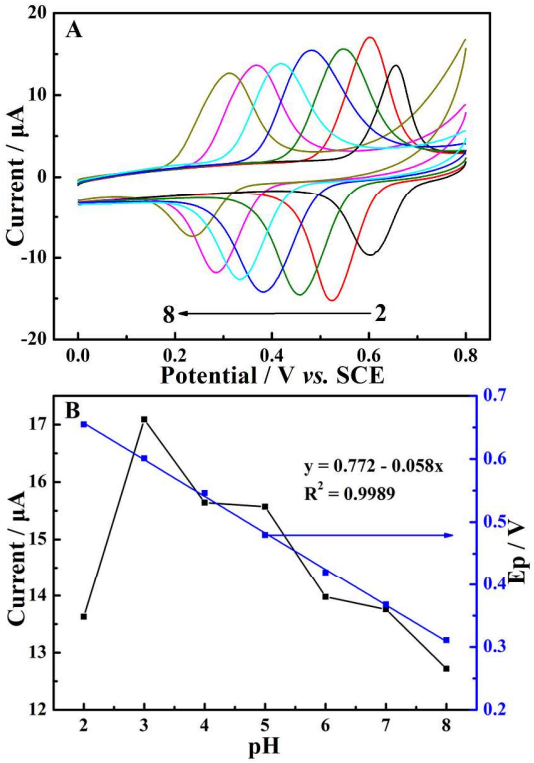

Fig. 5 (A) Cyclic voltammograms of Ni/GO-MWCNTs/GCE in presence of 50 μM luteolin in 0.1 M PBS, with different pH values: 2.0, 3.0, 4.0, 5.0, 6.0 .7.0 and 8.0. Scan rate: 50 mV s^{-1}. (B) Influences of pH on the oxidative peak current and oxidative peak potential.

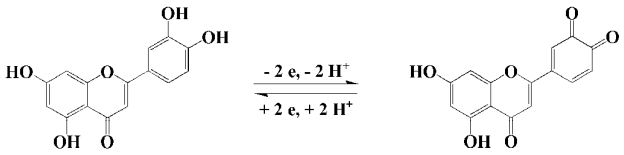

Scheme 2. The chemical structure and oxidation mechanism of luteolin

regression equations are expressed as E_{pa} = 0.4050 + 0.04605 ln v (mV s^{-1}), R^2 = 0.9789 and E_{pc} = 0.7921 - 0.05149 ln v (mV s^{-1}), R^2 = 0.9877. According to Laviron's model,[40] the slope of the line for E_{pa} and E_{pc} could be expressed as 2.303RT/(1 - α)nF and - 2.303RT/αnF, respectively. Therefore, the electrochemical parameters were calculated with the value of the electron-transfer coefficient (α) as 0.4721 and the electron-transfer number (n) as 2.427. Considering that the number of electron and proton involved in the luteolin oxidation process is equal, the electrooxidation of luteolin on Ni/GO-MWCNTs/GCE is a two-electron and two-proton process. The possible redox reaction mechanism can be expressed as Scheme 2.[16,19,41,42]

3.3.3 Effect of the accumulation time

It was believed that accumulation can improve the amount of luteolin absorbed on the electrode surface, and then improve determination sensitivity and decrease detection limit. Therefore, the influence of accumulation time on the oxidation behavior of 50 μM luteolin in 0.1 M PBS (pH 3.0) at Ni/GO-MWCNTs/GCE was investigated by DPV. As shown in Fig. 7, the oxidation peak currents of luteolin increased gradually with the accumulation time from 0 to 35 s. However, the oxidation peak currents increased slightly when further improving the accumulation time from 35 s to 65 s, suggesting that the amount of luteolin tended to a saturation on Ni/GO-MWCNTs/GCE. Considering both sensitivity and work efficiency, 35 s was employedin the further experiments.

3.3.4 Effect of the deposition time

Fig. 8 shows the relationship between the peak currents of luteolin and the deposition time of Ni at -0.20 V for Ni/GO-MWCNTs/GCE. The peak current increased with the time between 2 and 6 s. When the deposition time was prolonged to 6 s, the peak current decreased. Consequently, the deposition time of 6 s was chosen in the following electrochemical analysis.

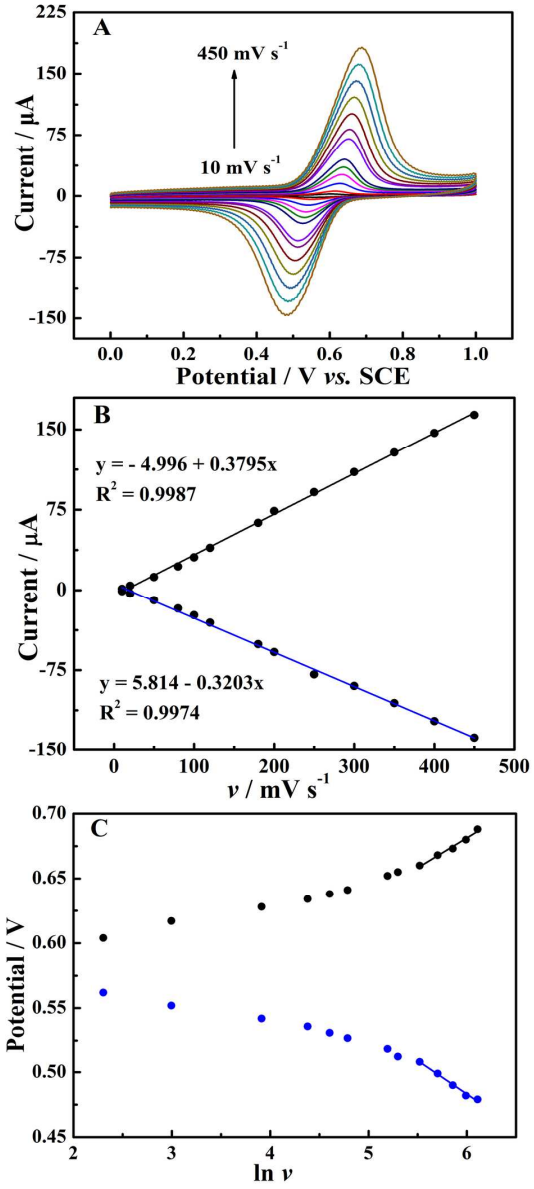

Fig. 6 (A) Cyclic voltammograms of Ni/GO-MWCNTs/GCE in presence of 50 μM luteolin in 0.1 M PBS (pH 3.0) with different scan rates (10, 20, 50, 80, 100, 120, 150, 180, 250, 300, 400, 450 mV s^{-1}). (B) The linear relationship of I_{pa} and I_{pc} with scan rates v (mV s^{-1}). (C) The relationship between the pick potentials and the Napierian logarithm of scan rate.

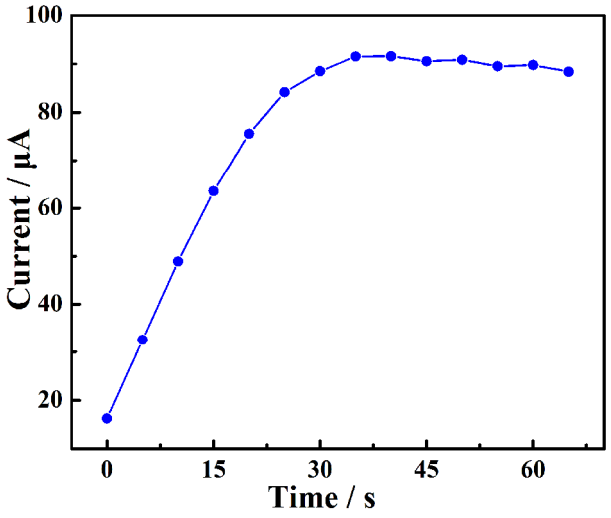

Fig. 7 Variation of the peak current with accumulation time presense of 50 μM luteolin in 0.1 M PBS (pH 3.0). Scan rate: 50 mVs^{-1}.

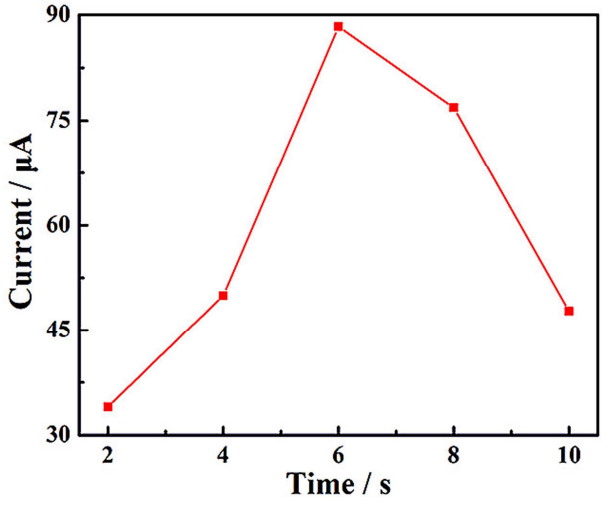

Fig. 8 The effects of deposition time on the reduction peak current of luteolin. The conditions are the presense of 50 μM luteolin in 0.1 M PBS (pH 3.0), Scan rate: 50 mV s^{-1}.

3.4. Chronocoulometry

For an adsorption controlled electrode process, it is necessary to calculate the saturated adsorptive capacity (Γ_{max}) of electroactivesubstance at the electrode surface. For getting the Γ_{max}, the active area (A) of electrode surface must be known first. The electrochemically effective surface areas (A) of bare GCE, Ni/GCE, GO/GCE, Ni-GO/GCE, GR/GCE, MWCNTs/GCE, Ni/GR/GCE, Ni/MWCNTs/GCE, GO-MWCNTs/GCE and Ni/GO-MWCNTs/GCE were determined by chronocoulometry using 0.1 mM $K_3[Fe(CN)_6]$ as model complex (the diffusion coefficient of $K_3[Fe(CN)_6]$ in 1 M KCl is 7.6×10^{-6} cm^2 s^{-1})[43] based on Anson equation:[44]

$$Q(t) = \frac{2nFAc(Dt)^{1/2}}{\pi^{1/2}} + Q_{dl} + Q_{ads}$$

where n is the numberof moles (n = 1), F is a Faraday constant (96485 C mol^{-1}), A is the surface area of working electrode, c is the concentration of luteolin (0.1 mM), D is the diffusion coefficient, Q_{dl} is double layer charge which could be eliminated by background subtraction, and Q_{ads} is Faradic charge. Other symbols have their usual meanings. Based on the slopes of the linear relationship between Q and $t^{1/2}$ (Fig. 7B), A was calculated to be 0.164 cm^2 (bare GCE), 0.367 cm^2 (Ni/GCE), 0.417 cm^2 (GR/GCE), 0.440 cm^2 (GO/GCE), 0.465 cm^2 (MWCNTs/GCE), 0.543 cm^2 (Ni/GO/GCE), 0.589 cm^2 (Ni/MWCNTs/GCE), 0.622 cm^2 (GO-MWCNTs/GCE) , 0.727 cm^2 (Ni/GR/GCE)and 0.783 cm^2 (Ni/GO-MWCNTs/GCE). It is obviously that the electrode effective surface areas of different dimensions substrates loading Ni are lager than those of pure substrates. Moreover, the electrode effective surface area of the Ni/GO-MWCNTs/GCE is 0.783 cm^2, which is obviously lager than those of Ni/GO/GCE (0.543 cm^2), Ni/GR/GCE (0.589 cm^2) and Ni/MWCNTs/GCE (0.727 cm^2), which would increase the electrochemical active site of luteolin, enhance the electrochemical response, and decrease the detection limit.

Furthermore,the saturated absorption capacity of luteolin on Ni/GO-MWCNTs/GCE was determined in 0.1 M PBS (pH 3.0) in the absence and presence of 0.1 mM luteolin (shown in Fig. 7C). According to the Q-t curves, the plots of Q against $t^{1/2}$ were made (inset of Fig. 7C). The slope of carve b' is 21.552×10^{-5} C $s^{-1/2}$ and the intercept (Q_{ads}) is 9.685×10^{-5} C. Using Laviron's theory of $Q_{ads} = nFA\Gamma_s$, as n = 2, A = 0.783 cm^2 and F = 96485 C mol^{-1}, the adsorption capacity (Γ_s) value of luteolin was 6.41×10^{-10} mol cm^{-2} at Ni/GO-MWCNTs/GCE.

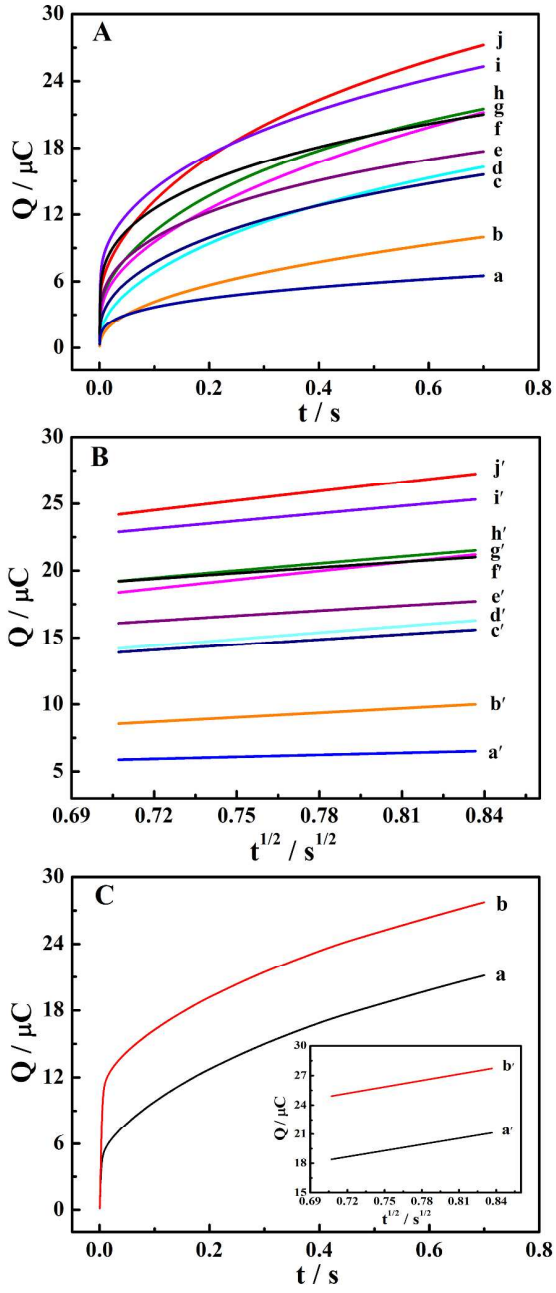

Fig. 9 (A) Plot of Q-t curves of (a) bare GCE, (b) Ni/GCE, (c) GO/GCE, (d) Ni/GO/GCE, (e) GR/GCE, (f) MWCNTs/GCE, (g) Ni/GR/GCE, (h) Ni/MWCNTs/GCE, (i) GO/MWCNTs/GCE, (j) Ni/GO-MWCNTs GCE in 0.1 mM $K_3[Fe(CN)_6]$ containing 1.0 M KCl. (B) plot of Q-$t^{1/2}$ curves on (a') bare GCE, (b') Ni/GCE, (c') GO/GCE, (d') Ni/GO/GCE, (e') GR/GCE, (f') MWCNTs/GCE, (g') Ni/GR/GCE, (h') Ni/MWCNTs/GCE, (i') GO-MWCNTs/GCE, (j') Ni/GO-MWCNTs/GCE. (C) Plot of Q-t curves of Ni/GO-MWCNTs/GCE in 0.1 M PBS (pH = 3.0) (a) in the absence and (b) presence of 100 μM luteolin. Insert: plot of Q-$t^{1/2}$ curve (a') in the absence and (b') presence of 100 μM luteolin.

3.5. Determination of luteolin

As a highly sensitive and a low detection limit electrochemical method, DPV was performed to investigate the relationship between the reduction peak current and the concentration of luteolin at the proposed electrochemical sensor under the optimal conditions. As shows in Fig. 10, the typical DPV obtained from different luteolin concentrations at Ni/GO-MWCNTs/GCE, Ni/GR/GCE and Ni/MWCNT/GCE in 0.1 M PBS(pH 3.0), and peak currents were proportional to the concentration of luteolin. The regression equation, correlation coefficient, linear range, and detection limit (S/N = 3) were summarized in Table 1. It can be observed that the Ni/GO-MWCNTs/GCE has wider linear range and lower detection limit, which can be attributed to higher electrocatalytic activity and larger active surface area, resulted from the unique 3D network structure. Table 2 gives the comparison of some of the analytical parameters obtained for luteolin in this study with other previous literatures. It can be seen the detection limit provided by this method is much lower than that reported in the literature. The comparison thus indicates that Ni/GO-MWCNTs composites are excellent sensing materials for the construction of electrochemical sensor for luteolin.

3.6. Reproducibility, stability and selectivity of Ni/GO-MWCNTs/GCE

The reproducibility of the modified electrode for the determination of a 20 μM luteolin was investigated. The relative standard deviation (RSD) was 3.96 % for 20 successive measurements, indicating an excellent reproducibility and precision. After the modified electrode was stored in refrigerator at 4 □ for 2 weeks, the DPV current response kept 89.37 % of its original response. The results demonstrated that the sensor exhibited excellent stability. The influences of some normal anions, cations and some other organic compounds were examined in the presence of 1 μMluteolin. It was found that 100-fold concentrations of K^+,

Na^+, Mg^{2+}, CO_3^{2-}, SO_4^{2-}; 50-fold glucose, dopamine, ascorbic acid; and 25-fold uric acid did not interfere the detection with the peak current changes less than ± 5%.

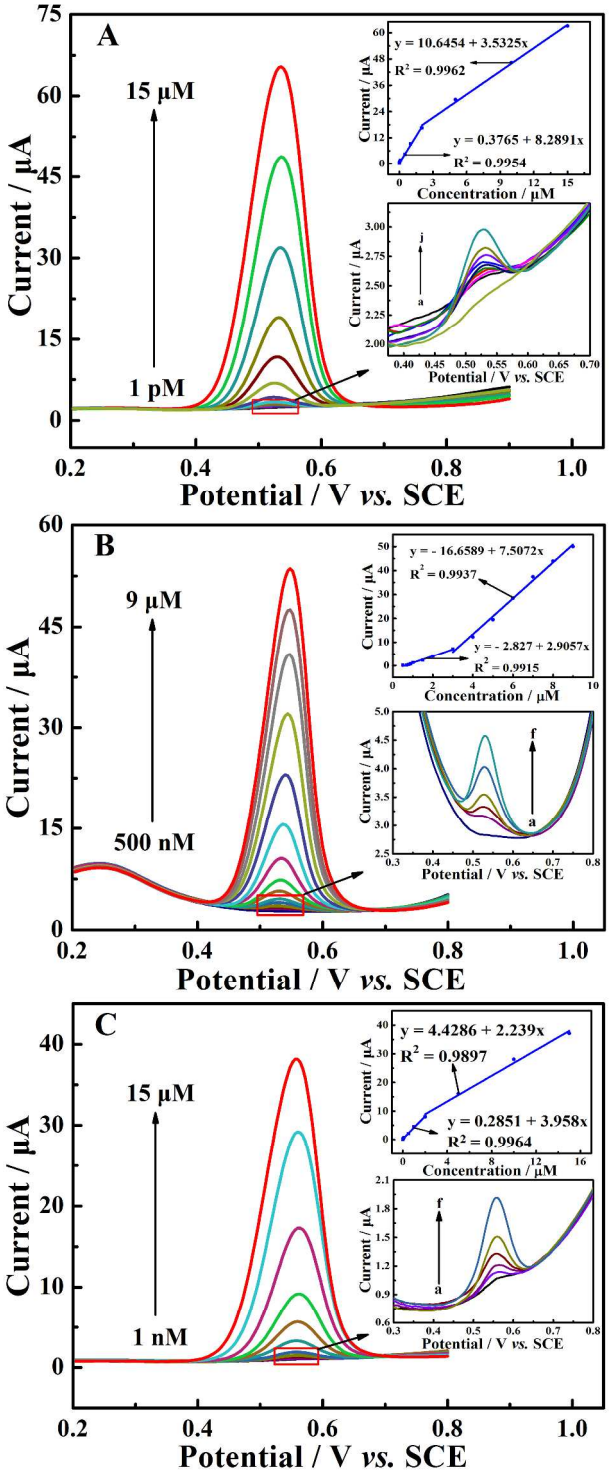

Fig. 10 (A) Typical DPV curves of different concentrations of luteolin on Ni/GO-MWCNTs/GCE in 0.1 M PBS (pH 3.0). Concentration of luteolin (a→j): 0, 0.001, 0.005, 0.01, 0.05, 0.1, 0.5, 1.00, 5.00, 10.00 nM. (B) Typical DPV curve of different concentrations of luteolin on Ni/GR/GCE in 0.1 M PBS (pH 3.0). Concentration of luteolin (a→f): 0, 0.5, 0.7, 0.8, 0.9, 1.0 μM. (C) Typical DPV curve of different concentrations of luteolin on Ni/MWCNT/GCE in 0.1 M PBS (pH 3.0). Concentration of luteolin (a→f): 0, 0.001, 0.005, 0.01, 0.05, 0.1 μM.

3.7. Determination of luteolin in *Lamiophlomis rotata Kudo capsules* and *peanut hulls*

Ni/GO-MWCNTs/GCE was further applied to determine luteolin in *Lamiophlomis rotata Kudo capsules* in PBS (3.0). Five capsules were finely powder was dissolved with ethanol. After sonication for 30 min and filtered into a beaker. Then, the clear filtrate was diluted with 0.1 M PBS (pH 3.0) to prepare the sample solutions. The samples were detected by the usual experimental procedure with the results shown in Table 3. The recovery was measured by the addition of the standard luteolin solution. It can be seen that the results were satisfactory with the recovery in the range of 99.03-101.44%, which indicated that the Ni/GO-MWCNTs/GCE couldbe efficiently used for the determination of luteolin content in *Lamiophlomis rotata Kudo capsules*.

Moreover, the method was further applied to the determination of luteolin in *peanut hulls*. Peanuts were purchased from a local market (Nanchang, China) and divided into hulls and edible parts. The *peanut hulls* were dried under room temperature and finely ground using a blender. The milled *peanut hulls* (50 mg) were extracted with 100 mL of ethanol at room temperature for 2 h. The sample was filtered with sand core funnel (10 μm) and distilled in a rotary evaporation and diluted to 100 mL with ethanol in a calibrated flask. A standard addition method was employed to evaluate the determination results. The analytical results were listed in Table 4 and the recovery was in the range of 97.96-102.22%, indicating that this method was reliable and feasible.

Table 1. Sensing Properties of Different Electrodes

Electrodes	Regression equation	R^2	Linear range	Detection
Ni/GO-MWCNTs/GCE	I_{pc}(μA) = 8.2891 c(μM) + 0.3765 and I_{pa}(μA) = 3.5325 c(μM) + 10.6454	0.9954 0.9962	1 pM--2 μM and 2 μM--15 μM	0.34 pM
Ni/GR/GCE	I_{pc}(μA) = 2.9057 c(μM) - 2.827 and I_{pa}(μA) = 7.5072 c(μM) - 16.6589	0.9915 0.9937	500 nM--3 μM and 3 μM--9 μM	167 nM
Ni/MWCNTs/GCE	I_{pc}(μA) = 3.958 c(μM) + 0.2851 and I_{pa}(μA) = 2.239 c(μM) + 4.4286	0.9964 0.9897	1 nM--2 μM and 2 μM--15 μM	0.34 nM

Table 2. Comparison of the analytical parameters for the luteolin detection on different electrodes.

Electrode	Linear range (mol L^{-1})	Detection limit (mol L^{-1})	Ref
MPC[a]/GCE	3.0×10^{-7} - 3.0×10^{-5}	1.3×10^{-9}	2
MWCNTs[b]/GCE	2.0×10^{-10} - 3.0×10^{-9}	6.0×10^{-11}	16
CS-GR[c]/GCE	2.0×10^{-9} - 1.0×10^{-6}	5.93×10^{-10}	17
PEDOT/EDTA-Ni[d] modified GCE	1.0×10^{-9} - 1.0×10^{-5}	3.0×10^{-10}	18
GNs/HA/[e]GCE	2.0×10^{-8} - 1.0×10^{-5}	1.0×10^{-8}	19
MWCNTs-BMIPF$_6$[f]/GCE	5.0×10^{-9} - 1.0×10^{-6}	5.0×10^{-10}	20
Au-BMI- PF$_6$ biosensor[g]	9.9×10^{-8} - 5.825×10^{-6}	2.8×10^{-8}	41
PDDA-G-CNTs/β-CD/[h]GCE	5.0×10^{-8} - 6.0×10^{-5}	2.0×10^{-8}	42
Ni/GO-MWCNTs/GCE	1.0×10^{-12} - 1.5×10^{-5}	3.4×10^{-13}	This work

[a] Macroporous carbon.

[b] Multi-walled carbon nanotubes.

[c] chitosan-graphene.

[d] poly(3,4-ethylenedioxythiophene)/ethylenediaminetetraacetic acid-Ni^{2+}.

[e] Graphene nanosheets and hydroxyapatite nanocomposite.

[f] multi-walled carbon nanotubes-ionic liquid (1-butyl-3-methylimidazolium hexafluorophosphate) composite.

[g] Au nanoparticle-1-butyl-3-methylimidazolium hexafluorophosphate modified carbon paste electrode.

[h] Poly(diallyldimethylammonium chloride)-functionalized graphene sheets-multiwalled carbon nanotubes/β-cyclodextrin.

Table 3. Determination of luteolin in *Lamiophlomis rotata Kudo*.

Samples	Detected (μmol L^{-1})	Added (μmol L^{-1})	Found (μmol L^{-1})	Recovery (%)
1	9.27	5.00	14.32	100.35
2	9.49	5.00	14.68	101.31
3	9.36	5.00	14.22	99.03
4	9.56	5.00	14.77	101.44
5	9.43	5.00	14.35	99.45

Table 4. Determination of luteolin in *peanut hulls*.

Samples	Detected(μmolL^{-1})	Added(μmolL^{-1})	Found(μmolL^{-1})	Recovery(%)
1	0.88	5.00	5.86	99.66
2	0.85	5.00	5.98	102.22
3	0.91	5.00	5.85	98.98
4	0.84	5.00	5.92	101.36
5	0.89	5.00	5.77	97.96

4. Conclusions

In summary, we developed a facile and effective method to fabricate a new type of composite electrode based on the electrochemical deposition of uniform Ni clusters on 3D porous GO-MWCNTs supporting matrix. Enormous amount of work has been done on the application of for electrochemical applications. However, pristine MWCNTs are highly hydrophobic and as a result it is impossible to prepare their stable aqueous dispersion. In this work, hydrophilic GO was used as a superior dispersant to disperse MWCNTs. The nanocomposite of MWCNTs and GO could significantly reduce the aggregation and stacking between MWCNTs, which resulted in enhanced surface area and 3D interconnect structure of GO-MWCNTs. The obtained Ni/GO-MWCNTs electrode exhibites larger electrochemical active surface area, better electrocatalytic activity and stability for the oxidation of luteolin than Ni/GR, and Ni/MWCNTs composites, which enable it to be used as sensitive electrochemical sensor for the detection of luteolin. Under the optimized conditions, the proposed sensor can be applied to the quantification of luteolin with a wide linear range covering from 1 pM to 15 μM with a low detection limit of 0.34 pM (S/N = 3). The proposed method was further applied to the determination of luteolin in Lamiophlomis rotata Kudo capsules and peanut hulls with satisfactory results. The 3D Ni/GO-MWCNTs composite, with easy synthesis, simple manufacturing process and high performance, holds great promise for the practical application in electrochemical sensor.

Acknowledgements

We are grateful to the National Natural Science Foundation of China (51302117, 51463008, 51272096 and 51263010), Ganpo Outstanding Talents 555 projects, Jiangxi Provincial, Department of Education (GJJ12595, GJJ13565 and GJJ13258), Natural Science Foundation of Jiangxi Province (20151BAB203018), Postdoctoral Science Foundation of China (2014M551857 and 2015T80688), Postdoctoral Science Foundation of Jiangxi Province (2014KY14), Youth Science and Technology Talent Training Plan of Chongqing Science and Technology Commission (CSTC2014KJRC-QNRC10006) for their financial support of this work.

Notes and references

[a] Jiangxi Key Laboratory of Organic Chemistry, Jiangxi Science & Technology Normal University, Nanchang, 330013, China

[b] College of Science, Jiangxi Agricultural University, Nanchang 330045, China

* Corresponding Author: Prof. Dr. Jingkun Xu

Fax: +86-791-83823320; tel.:+86-791-88537967. E-mail: xujingkun@tsinghua.org.cn.

* Corresponding Author: Dr. LiminLu

Fax: +86-791-83813048; tel.: 86-791-83813048. E-mail: lulimin816@hotmail.com;

1 N. K. Peters, J. W. Frost and S. R. Long, *Science*., 1986, **233**, 977-980.

2 L. J. Zeng, Y. F. Zhang, H. Wang and L. P. Guo, *Anal. Methods*., 2013, **5**, 3365-3370.

3 Y. J. Park, H. J. Kim, S. J. Lee, H. Y. Choi, C. Jin and Y. S. Lee, *Chem.Pharm. Bull*., 2007, **55**, 1065-1066.

4 G. H. Cao, E. Sofic and R. L. Prior, *Free Radical Biol. Med*., 1997, **22**, 749-760.

5 M. G. Hertog, E. J. Feskens, P. C. Hollman, M. B. Katan and D. Kromhout, *Lancet*, 1993, **342**, 1007.

6 P. Knekt, R. Jarvinen, A. Reunanen and J. Maatela, *Br. Med. J.*, 1996, **312**, 478-481.

7 M. G. L. Hertog, D. Kromhout and C. Aravanis, *Arch. Intern. Med.*, 1995, **155**, 381-386.

8 L. P. Li and H. D. Jiang, *J. Pharm. Biomed. Anal.*, 2006, **41**, 261-265.

9 R. Benetis, J. Radusiene, V. Jakstas, V. Janulis, G. Puodziuniene and A. Milasius, *Pharm. Chem. J.*, 2008, **42**, 153-156.

10 R. J. Grayer, G. C. Kite, M. A. Zaid and L. J. Archer, *Phytochem. Anal.*, 2000, **11**, 257-267.

11 D. A. v. Elswijka, U. P. Schobel, E. P. Lansky, H. Irthc, J. v. d. Greef, *Phytochemistry.*, 2004, **65**, 233-241.

12 I. Baranowska and D. Raróg, *Talanta.*, 2001, **55**, 209-212.

13 Y. Y. Li, Q. F. Zhang, H. Y. Sun, N. K. Cheung and H. Y. Cheung, *Talanta.*, 2013, **105**, 393-402.

14. A. Baracco, G. Bertin, E. Gnocco, M. Legorati and S. Sedocco, *Rapid Commun Mass Spectrom.*, 1995, **9**, 427-436.

15 Y. S. Gao, L. P. Wu, K. X. Zhang, J. K. Xu, L. M. Lu, X F. Zhu and Y. Wu, *Chinese Chemical Letters.*, 2015, **26**, 613-618.

16 D. M. Zhao, X. H. Zhang, L. J. Feng, Q. Qi and S. F Wang, *Food Chem*., 2011, **127**, 694-698.

17 G. J. Li, L. H. Liu, Y. Cheng, S. X. Gong, X. L. Wang, X. J Geng and W. Sun, *Anal. Methods*, 2014, **6**, 9354-9360.

18 L. P. Wu, Y. S. Gao, J. K. Xu, L. M. Lu, and T. Nie, *Electroanalysis*., 2014, **26**, 2207-2215.

19 P. F. Pang, Y. P. Liu, Y. L. Zhang, Y. T. Gao and Q. F. Hu, *Sensors and Actuators B.*, 2014, **194**, 397-403.

20 J. Tang and B. K. Jin, *Anal. Methods.*, 2015, **7**, 894-900.

21 Y. Z. Chen, D. L. Peng, D. X. Lin and X. H. Luo, *Nanotechnology*, 2007, **18**, 505703.

22 A. Döner, E. Telli, G. Kardas, *Journal of Power Sources*., 2012, **205**, 71-79.

23 J. F. Sun, J. Q. Wang, Z. P. Li, L. Y. Niu, W. Hong,S. R. Yang , *Journal of PowerSources*., 2015, **274**, 1070-1075.

24 S. A. Needham, G. X. Wang, H. K. Liu, L. Yang, *J Nanosci Nanotechnol*., 2006, **6**, 77-81.

25 W. Zhou, L. J. Lin, D. Y. Zhao, and L. Guo, *J. Am. Chem. Soc*., 2011, **133**, 8389-8391.

26 Z. G. Wu, M. Munoz, O. Montero, *Advanced Powder Technology*., 2010, **21**, 165-168.

27 J. F. Xiong, H. Shen, J. X. Mao, X. T. Qin, P. Xiao, X. Z. Wang, Q. Wu and Z. Hu, *J. Mater. Chem*., 2012, **22**, 11927-11932.

28 L. Ren, K. S. Hui and K. N. Hui, *J. Mater. Chem. A*., 2013, **1**, 5689-5694.

29 K. Krishnamoorthy, R. Mohan and S. J. Kim, *Appl. Phys. Lett.*, 2011, **98**, 1-3.

30 P. D. Tran, L. H. Wong, J. Barberbcd and J. S. C. Loo, *Energy Environ. Sci*., 2012, **5**, 5902-5918.

31 Y. W. Zhu , S. Murali , W. W. Cai , X. S. Li, J. W. Suk , J. R. Potts and R. S. Ruoff, *Adv. Mater*., 2010, **22**, 3906-3924.

32 X. L. Wang, Y. Liu, S. Tao, B. S. Xing, *Carbon*, 2010, **48**, 3721-3728.

33 S. Cheemalapati, S. Palanisamy, V. Mani and S. M. Chen, *Talanta*., 2013, **117**, 297-304.

34 Y. Zhang, Z. Xia, H. Liu, M. J. Yang, L. L. Lin and Q. Z. Li, *Sensors and Actuators B*., 2013, **188**, 496-501.

35 L. Chen, X. J. Wang, X. T. Zhang and H. M. Zhang, J. Mater. Chem., 2012, 22, 22090-22096.

36 X. F. Zhu, L. M. Lu, X. M. Duan, K. X. Zhang, J. K. Xu, D. F. Hu, H. Sun, L. Q. Dong, Y. S. Gao and Y. Wu, *J. Electroanal. Chem.*, 2014, **731**, 84-92.

37 K. X. Zhang, L. M. Lu, Y. P. Wen, J. K. Xu, X. M. Duan, L. Zhang, D. F. Hu and T. Nie, *Analytica Chimica Acta.*, 2013, **787**, 50-56.

667 38 R. Rajendran, L. K. Shrestha, K. Minami, M. Subramanian,
668 R. Jayavel, and K. Ariga, *J. Mater. Chem. A.*, 2014, **2**,
669 18480-18487.
670 39 H. R. Zare, Z. Sobhani and M. M.Ardakani, *Sensors and*
671 *Actuators B*., 2007, **126**, 641-647.
672 40 E. Laviron, *J. Electroanal. Chem.*, 1979, **101**, 19-28.
673 41 A. C. Franzoi, I. C. Vieira, J. Dupont, C. W. Scheeren and L.
674 F. de Oliveira, *Analyst.*, 2009, **134**, 2320-2328.
675 42 D. B. Lu, S. X. Lin, L. T. Wang, T. Li, C. M. Wang and Y.
676 Zhang, *J. Solid. State. Electr.*, 2014, **18**, 269-278.
677 43 D. B. Lu, S. X. Lin, L. T. Wang, X. Z. Shi, C. M. Wang
678 and Y. Zhang, *Electrochimica Acta.*, 2012, **85**, 131-138.
679 44 F. C. Anson, *Anal. Chem.*, 1964, **36**, 932-934.
680
681